Total energy distributions of field-emitted electrons at high current density

A. E. Bell and L. W. Swanson
Oregon Graduate Center, Beaverton, Oregon 97005
(Received 29 September 1978)

Measurements of the total energy distributions (TED) have been carried out at high current densities ($J = 10^6$ to 10^8 A/cm^2) for a high-work-function ($\phi = 4.5$ eV) and low-work-function ($\phi = 2.5$ eV) field emitter. At high values of J, both emitters give values of the full width at half maximum (FWHM) of the TED which exceed the values based on Fowler-Nordheim theory by a few eV. This deviation of the FWHM values increases with J, is independent of temperature, and decreases with emitter radius for a specified beam acceptance angle. The study of these anomalous values of FWHM values extends from 84 to 1975 K. It is believed that Coulomb interaction in the vacuum space in front of the emitter can account for these results, although internal electron energy-broadening mechanisms cannot be ruled out.

I. INTRODUCTION

In this study, we report an anomalous broadening of the total energy distribution (TED) of field-emitted electrons at high current density. Previous investigators have noted various deviations in the TED of field-emitted electrons from clean metal surfaces.[1–5] The deviations referred to are those experimental TED results which do not follow the theory put forth by Fowler and Nordheim[6] (FN), based on the Sommerfeld free-electron model of the solid and later modified to include the effect of temperature.[7] Such deviations observed in the TED include (i) those due to alteration of the substrate local density of states due to bulk band structure[8,9] or surface adsorption[10,11]; (ii) relaxation processes involving electron scattering in the bulk[3,12,13]; and (iii) energy broadening due to tunneling lifetimes.[14]

For the most part, the TED deviations referred to above consist of relatively small perturbations that require sensitive electron spectrometers for their detection and have no detectable effect on the current-voltage $I(V)$ characteristics as analyzed by so-called FN plots, and have little effect on the value of the full width at half maximum (FWHM). Recently, it was reported that a significant broadening (i.e., increase in the FWHM of the TED beyond theoretical expectation) occurred when field emitters were operated in the thermal-field (TF) mode at high current-density $J > 10^6$ A/cm^2.[15] In addition, this anomalous increase in FWHM of the TED was accompanied by deviations in the FN plot, which had been observed earlier,[16] and an unusual reduction in the $1/f$ noise amplitude.

The purpose of this investigation was to study the effect of such parameters as emitter size, current density, temperature, work function, and beam acceptance angle on the FWHM of TED measurements taken at large values of J. In order to perform TED measurements at elevated temperatures without the problem of unpredictable, time-dependent change of the emitter shape due to field-induced buildup processes, two emitters of different work function that are known to be stable at elevated temperature were used in this study. Both emitters were (100)-oriented tungsten — the low-work-function one was a zirconium-coated Zr-W(100) emitter[15,17,18] and the high-work-function one was a W(100) builtup[15,17,19] emitter. These emitters are capable of high-J operation over the temperature range 78 to 1900 K, and confine the emission to an 8° half angle. The angular confinement occurs through selective lowering of the (100) work function in the case of the Zr-W(100) emitter and by local-field enhancement in the case of the W(100) builtup emitter.

Besides the general interest in characterizing and understanding the TED broadening phenomenon, there is further interest regarding its effect on the use of field-emission (FE) sources in a growing number of microprobe applications. Both of the FE sources investigated in this study are capable of long-lived dc operation at angular intensities in excess of 1 mA/sr. However, the enhanced broadening of the TED will cause chromatic aberration to become a dominant factor limiting the spot size of a focused beam.

In Sec. II, the FE sources and method of measurement are described in further detail. Secs. III and IV describe the experimental techniques and results. In Sec. V, a discussion of the results and possible mechanisms explaining the enhanced TED are presented. We conclude that a possible mechanism involves collective Coulomb interaction between the emitted electrons similar to that proposed by Loeffler,[20] Zimmerman,[21] and others[22] to explain the TED broadening noted by Boersch[23] at beam crossovers. However, certain electron energy-broadening

mechanisms occurring in the bulk cannot be ruled out as contributing to the anomalous TED broadening reported here.

II. METHOD OF APPROACH

Based on the Sommerfeld model of metals, the TED of field-emitted electrons is given by

$$J(\epsilon) = \left(\frac{4\pi me}{h^3}\right) f(\epsilon) \int_0^{E_F+\epsilon} D(W)\, dW \ , \qquad (1)$$

where $\epsilon = E - E_F$ is the total electron energy relative to the Fermi level E_F, and W is the kinetic energy associated with the component of momentum perpendicular to the surface. The term $f(\epsilon)$ is the Fermi function

$$f(\epsilon) = 1/[1 + \exp(\epsilon/kT)] \ ,$$

while $D(W)$ is the one-dimensional transmission function which is obtained from[24]

$$D(W) = (1 + e^{A(W)})^{-1} \qquad (2)$$

where

$$A(W) = \frac{4}{3}\left(\frac{2m}{\hbar^2}\right)^{1/2} \frac{E_F + \phi - W)^{3/2}}{eF} v(y) \ ,$$

in which ϕ and F are the work function and electric field.

When TED measurements are made at low temperatures and examined in an energy range extending no more than a few tenths of an eV on either side of the Fermi level, then it may be adequately represented by the simple expression

$$J(\epsilon) = (J_0/d) f(\epsilon) \exp(\epsilon/d) \ , \qquad (3)$$

where

$$d = \hbar eF/2(2m\phi)^{1/2} t(y) \qquad (4)$$

and J_0 is the 0-K FN relation

$$J_0 = \frac{e^3F^2}{8\pi h \phi t^2(y)} \exp\left(\frac{-4(2m\phi^3)^{1/2} v(y)}{3\hbar eF}\right) \ , \qquad (5)$$

where $v(y)$ and $t(y)$ are tabulated correction terms due to the image potential, and are explained in detail elsewhere.[7]

The approximate expression for $J(\epsilon)$ given in Eq. (3) is accurate for $p = kT/d < 0.7$. However, for $p \gtrsim 0.7$ the approximations used in deriving Eq. (3) break down and the TED must be evaluated by numerically integrating Eq. (1). El-Kareh, Wolfe, and Wolfe[25] have carried out the numerical integration of Eq. (1) over the complete temperature-field and work-function range; in addition, they along with others[26] performed the integration

$$J(T,F) = \int_0^\infty J(\epsilon)\, d\epsilon \ , \qquad (6)$$

which gives the current density over the complete range of the variables T, F, and ϕ. Equation (5) is the result of performing the integration of Eq. (6) at $T = 0$.

Equations (1) and (6) were evaluated at $\phi = 2.5$ and 4.5 eV using the numerical integration techniques described elsewhere.[25] These are the work-function values appropriate for the Zr-W(100) and W(100) builtup emitters investigated in this study. Figures 1 and 2 give the relationship between the FWHM and F. The arrows on the ordinate indicate the electric-field range applicable to the respective emitters. The origin of the maxima in the FWHM curves is as follows: at high fields, emission is dominated by emission from the vicinity of the Fermi level, whereas at low fields, it is confined to the top of the work-function barrier. On the other hand, at intermediate fields, comparable emission occurs in the region of the Fermi level and the top of the work-function barrier leading to the maxima in Figs. 1 and 2 curves. The maxima in Figs. 1 and 2 curves are largest for the high work-function emitter; however, except for $T > 1800$ K, they lie outside the field range of interest.

We thus conclude that in the field and temperature range of interest for the two emitters investigated in this study, the FWHM should not exceed ~ 1 eV. Previous studies by Gadzuk and Plummer[27] and others[1,3] have shown that for low-field strengths and a temperature range extending from 78 to 1500 K, a tungsten emitter gave TED results in agreement with theoretical expectations, except for the well-known structure in the W(100) TED that occurs at $\epsilon = -0.35$ and -0.70 eV.

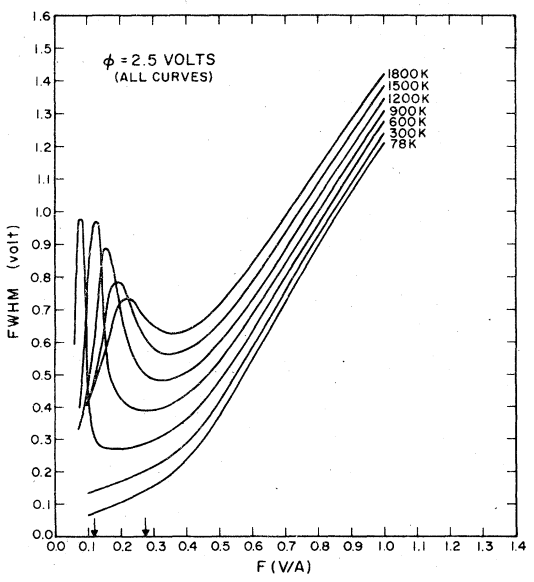

FIG. 1. Plot of theoretical values of FWHM for the energy distribution of field-emitted electrons as a function of electric-field F at various temperatures; work function is 2.5 eV.

The two emitters chosen for this study, besides their capability of being operated at temperatures up to 1900 K, can also be operated at very high values of current density. The latter feature arises from the fact that both emitters confine the emitting area to less than 10% of the normal state. The Zr-W(100) emitter confines the emitting area by a thermally-stable adsorbed layer of ZrO which specifically lowers the work function of the (100) crystal plane.[17,18] In contrast, the W(100) builtup emitter causes a similar confinement of the emitting area, but by a local-field enhancement due to a field-induced faceting of the {112} and {110} planes.[17,19,28] The thrust of our study was to measure the FWHM values of the TED curves obtained from these two emitters and compare the results with Figs. 1 and 2 predictions. In particular, we measured the TED curves obtained from these two emitters for higher values of J than have heretofore been examined.

III. EXPERIMENTAL

Two retarding potential analyzers were used in this study, one of which has been described earlier[1] and involves focusing the emitted electrons to a crossover at the center of a retarding hemisphere; the other analyzer employed was a noncrossover retarding analyzer in which the electrons are retarded along radial paths by concentrically-arranged spherical electrodes. A cross section of the latter analyzer is depicted in Fig. 3 and Table I gives the radii and relative operating potentials of the electrodes. Electrode potentials were determined according to

$$\frac{V(r)}{V(r_0)} = 1 - \frac{R}{R - r_0}\left(1 - \frac{r_0}{r}\right), \tag{7}$$

where r_0 is the inner-sphere radius and R is the outer-sphere radius. In practice, the best resolution was obtained if the potential of electrode D was 0.03 $V(r_0)$ and electrode E was operated at 3 V. A negative sweep potential was applied to the emitter in order to display the retarding current-voltage characteris-

TABLE I. Spherical retarding analyzer electrode specification based on Eq. (7).

Electrode	Inner Radius (mm)	Aperture Diameter (mm)	Relative Voltage
A	3.96	3.05	1.0
B	10.54	0.71	0.264
C	14.10	0.71	0.164
D	20.27	0.71	0.060
E	30.38	3.81[a]	0.0

[a]Covered by 1000-lines/in. copper mesh.

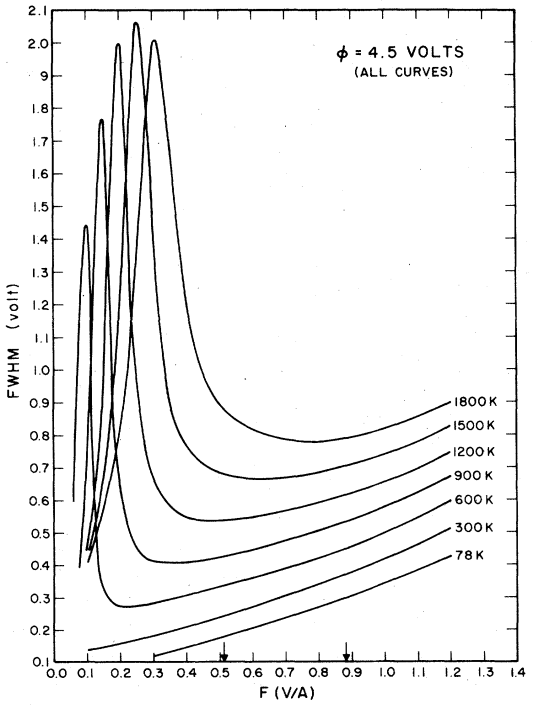

FIG. 2. Plot of theoretical values of FWHM for the energy distribution of field-emitted electrons as a function of electric-field F at various temperatures; work function is 4.5 eV.

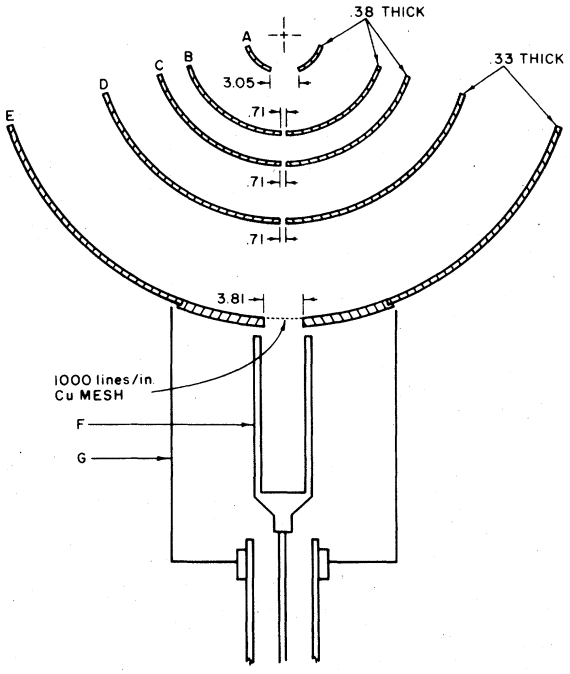

FIG. 3. Diagram of the electrode configuration for the noncrossover retarding electron energy analyzer. Dimensions in mm.

tics. The selecting electrode (E) contained a 1000-line/in. platinum-coated copper mesh through which electrons were transmitted into the Faraday collector (F). The emitter was mounted on a glass-bellows arrangement in order to align it with the spherical electrodes. For best resolution, the emitter was positioned 0.56 mm behind the center of symmetry of the hemispherical electrodes. A fluorescent screen on electrode (B) was provided for pattern observation. The resolution of this analyzer was ~ 50 meV, as determined from the leading edge of the TED taken at an emitter temperature of 78 K.

Both electron energy analyzers directly yielded the integral of the FE current with respect to the electron energy; this was differentiated electronically to provide the TED. At elevated temperature, the extent to which the TED measurements could be carried out along the low-energy tail was limited by beam noise. Temperature control of the emitter was accomplished by the well-known 4-lead emitter assembly where two small diameter (~ 0.1 mm) leads sample the emitter filament resistance. Temperature calibration for $T > 1000$ K was performed using an optical pyrometer, while temperature calibration for $T < 1000$ K was accomplished by using the resistivity-temperature dependence relationship for pure tungsten.

The two electron energy analyzers were mounted on bakable, high-vacuum systems capable of attaining a pressure $< 8 \times 10^{-10}$ Torr. Because of the high total-electron-current levels used in this study, electron-stimulated desorption of absorbed gases on the anode limited the effective pressure at the emitter. This problem could be reduced to a tolerable level by operating the emitter for several hours at high current level prior to taking TED measurements.

IV. EXPERIMENTAL RESULTS

Measurements of the TED curves were carried out as a function of T, F, β, and beam-aperture angle. The field factor $\beta = F/V$ was determined in the usual way from the slope of the low-temperature FN plot [i.e., $\ln(I/V^2)$ vs $1/V$] by assuming the previously stated ϕ values. The beam acceptance angle was the solid angle (Ω) subtended at the emitter by the

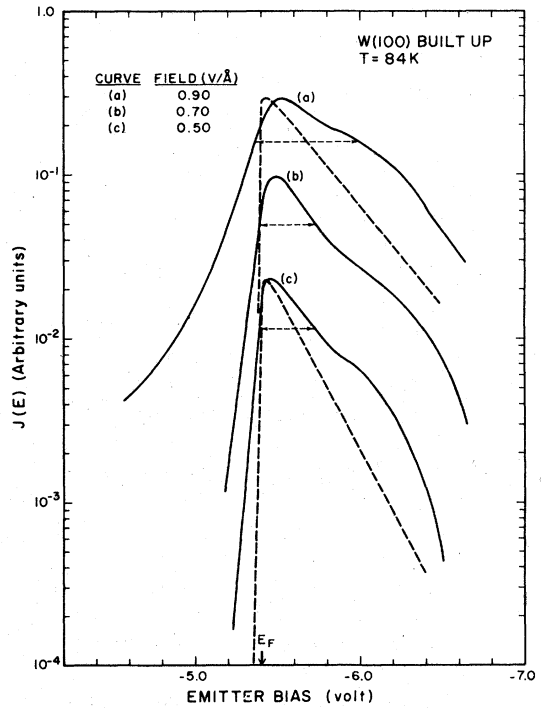

FIG. 4. Solid lines are the experimental TED curves for a W(100) builtup emitter taken at the indicated electric fields and temperature; dashed lines are the corresponding theoretical curves using $\phi = 4.5$ eV, and normalized to the peak heights and Fermi-level E_F of the respective experimental curves. Horizontal dashed lines indicate the experimental FWHM values. Crossover analyzer with $\Omega = 0.14$ msr used for these results.

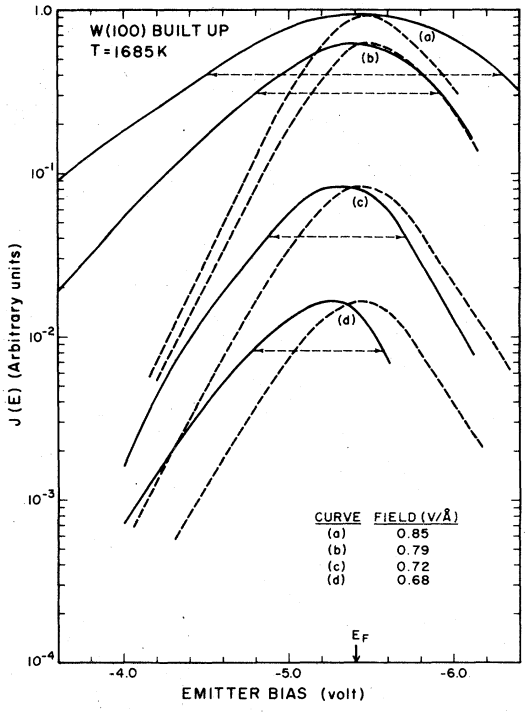

FIG. 5. Solid lines are the experimental TED curves for a W(100) built-up emitter taken at the indicated electric fields and temperature; dashed lines are the corresponding theoretical curves using $\phi = 4.5$ eV and normalized to the peak heights and Fermi-level E_F of the respective experimental curves. Horizontal dashed lines indicate the experimental FWHM values. Crossover analyzer with $\Omega = 0.14$ msr used for these results.

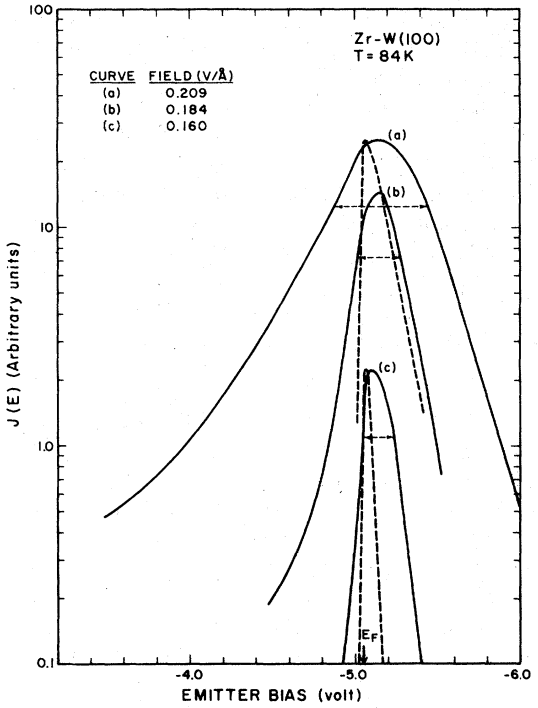

FIG. 6. Solid lines are the experimental TED curves for a Zr-W(100) emitter taken at the indicated electric fields and temperature; dashed lines are the corresponding theoretical curves using $\phi = 2.5$ eV and normalized to the peak heights and Fermi-level E_F of the respective experimental curves. Horizontal dashed lines indicate the experimental FWHM values. Crossover analyzer with $\Omega = 0.14$ msr used for these results.

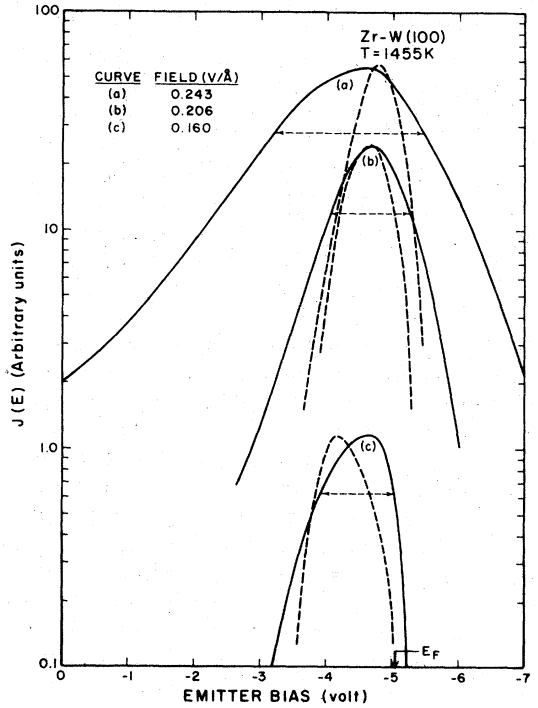

FIG. 7. Solid lines are the experimental TED curves for a Zr-W(100) emitter taken at the indicated electric fields and temperature; dashed lines are the corresponding theoretical curves using $\phi = 2.5$ eV and normalized to the peak heights and Fermi-level E_F of the respective experimental curves. Horizontal dashed lines indicate the experimental FWHM values. Crossover analyzer with $\Omega = 0.14$ msr used for these results.

beam-defining aperture. The "crossover" analyzer was operated with two different apertures giving $\Omega = 0.14$ and 0.54 msr, while the noncrossover analyzer was operated with one aperture size giving $\Omega = 0.97$ msr.

Figures 4 to 7 show the experimental TED curves obtained from the crossover energy analyzer for the W(100) built up and Zr-W(100) emitters at various values of F, and two extreme values of T. A few of the theoretical curves normalized to the respective experimental-curve peak heights are given for comparison purposes. Figures 8 and 9 give the comparison between the experimental and theoretical values of FWHM for the Figs. 4 to 7 data. A large discrepancy can be seen between experiment and theory at large values of F for both high and low temperatures.

Figure 10 shows the high-temperature FWHM values for the W(100) built-up emitter taken in the crossover analyzer with a larger beam-acceptance angle ($\Omega = 0.54$ msr), and at various values of emitter radii. The FWHM values are given in terms of the beam angular intensity in order to show its dependence on the latter parameter. Figure 11 gives similar results for a W(100) builtup emitter with approximately the same emitter radius r (i.e., similar values of β, where we have $\beta \propto 1/r$) but at various beam acceptance angles. The values for $\Omega = 0.97$ msr in Fig. 11 were obtained from the noncrossover analyzer, as were the results in Fig. 12, which were taken with a smaller β value emitter at several temperatures. Figures 10 to 14 results show that in the temperature range investigated, the FWHM values are independent of temperature and primarily a function of β, Ω, and angular beam intensity.

In Fig. 13 the FWHM values versus angular intensity are given for the Zr-W(100) emitter at various temperatures using the crossover analyzer with two different beam acceptance angles. The indicated theoretical curves were obtained from Figs. 1 and 2 data, using the experimental values of β and anode voltage to obtain the appropriate value of F and, hence, FWHM values.

Finally, in Fig. 14 are the values of FWHM vs β

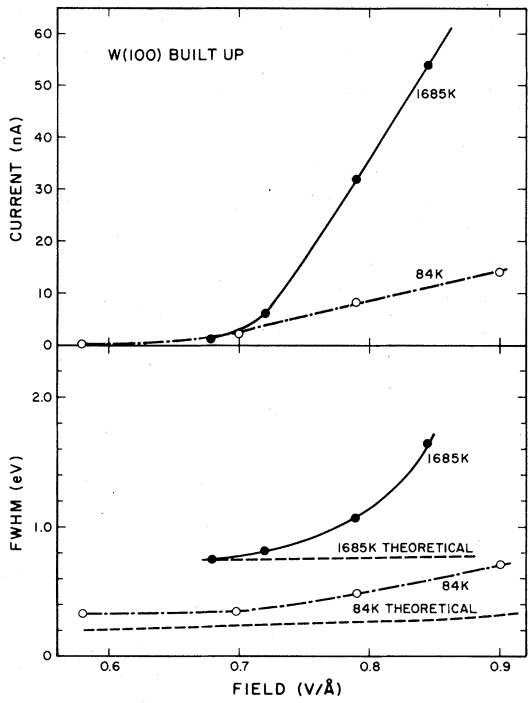

FIG. 8. Solid and dot-dashed lines are the experimental values of transmitted current (upper figure) and FWHM values vs electric field (lower figure). Results correspond to Figs. 4 and 5 data. Dashed lines (lower figure) are theoretical values of FWHM.

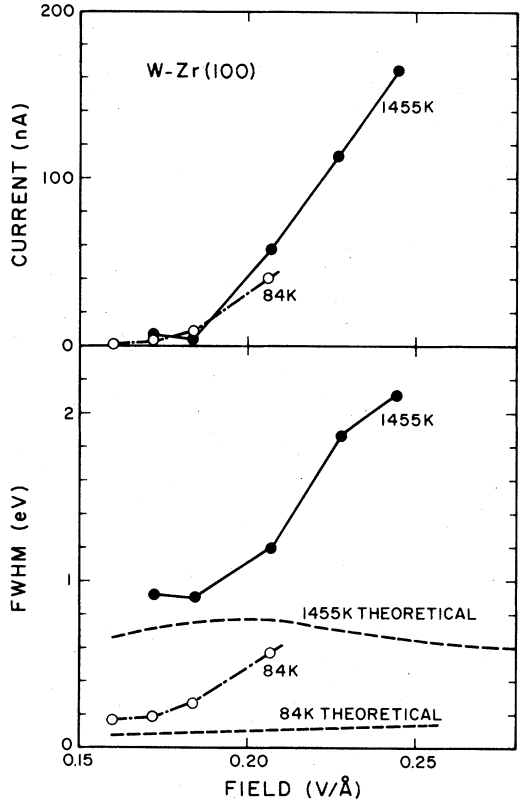

FIG. 9. Solid and dot-dashed lines are the experimental values of transmitted current (upper figure) and FWHM values vs electric field (lower figure). Results correspond to Figs. 6 and 7 data. Dashed lines (lower figure) are theoretical values of FWHM.

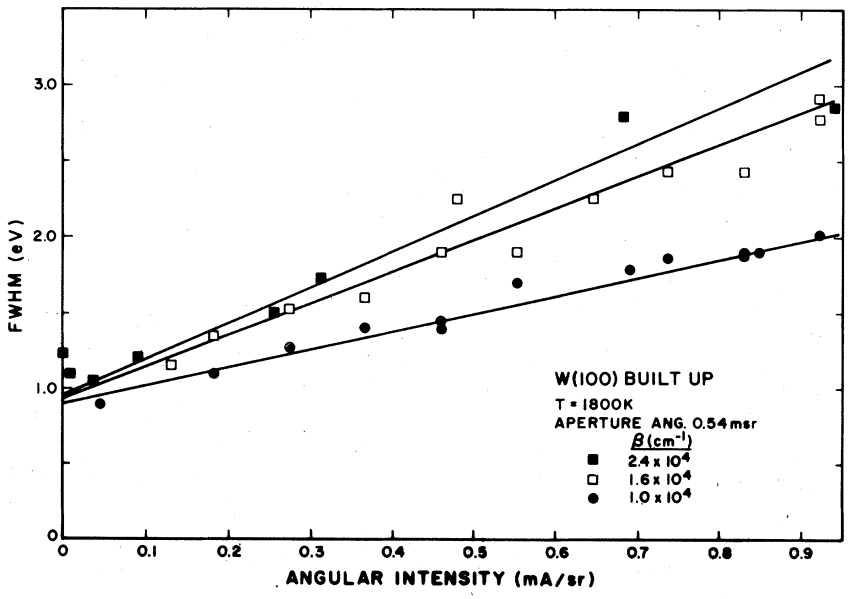

FIG. 10. Experimental values of FWHM vs beam angular intensity for three W(100) builtup emitters with the indicated values of emitter field factor β. Data obtained from the crossover analyzer with $\Omega = 0.54$ msr.

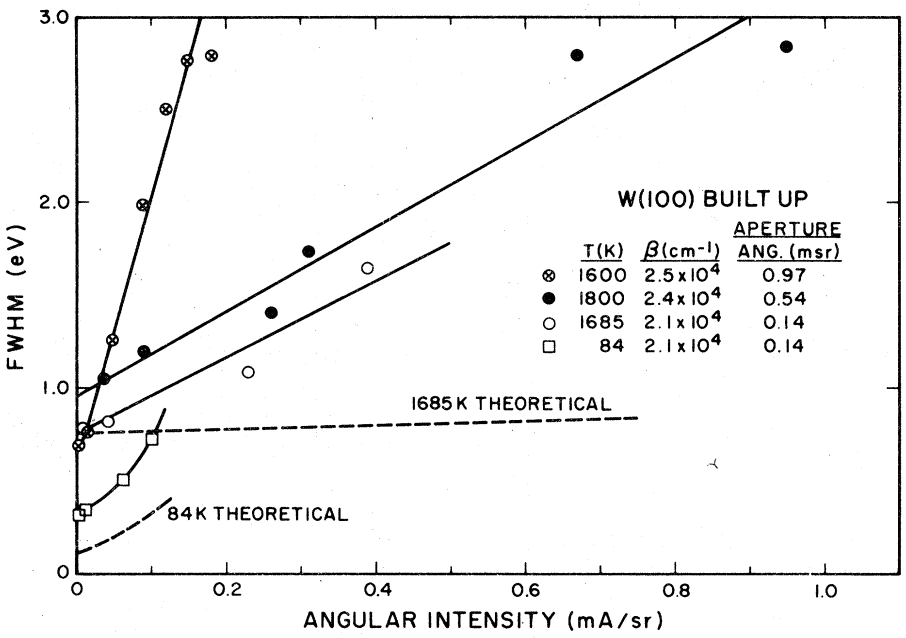

FIG. 11. Experimental values of FWHM vs beam angular intensity for the W(100) builtup emitter at various values of beam acceptance angle Ω. Values for $\Omega = 0.97$ msr are obtained from the noncrossover analyzer; other values of Ω are taken from crossover analyzer. Dashed lines are theoretical curves for the 84- and 1685-K data.

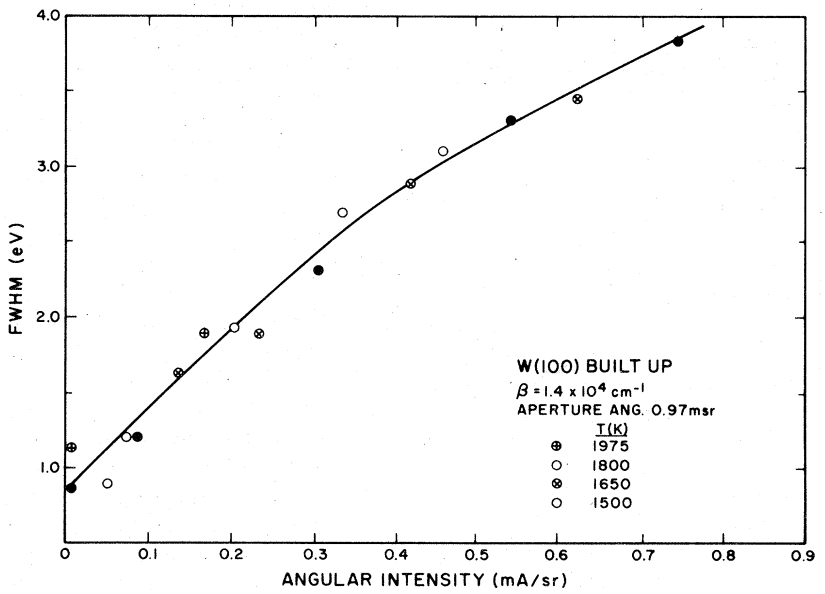

FIG. 12. Experimental values of the FWHM vs beam angular intensity for a W(100) builtup emitter at the indicated temperatures using the noncrossover analyzer.

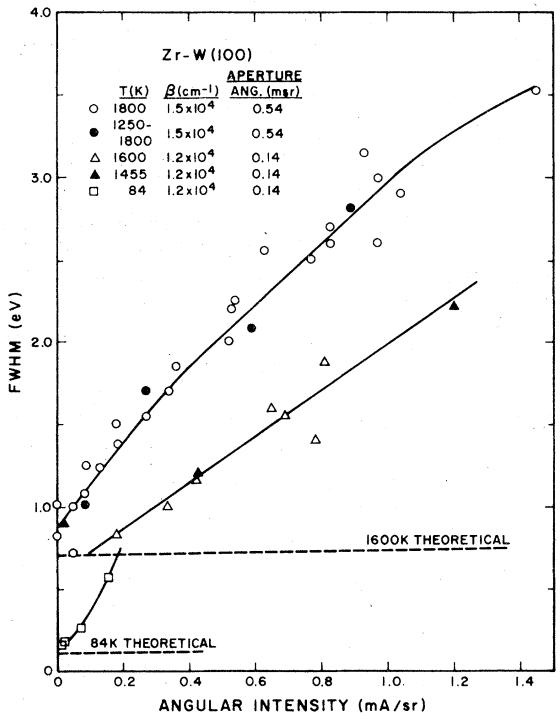

FIG. 13. Experimental values of FWHM vs beam angular intensity for the Zr-W(100) emitter at two values of beam acceptance angle Ω. Data obtained from crossover analyzer. Dashed lines are theoretical curves for 84- and 1600-K data.

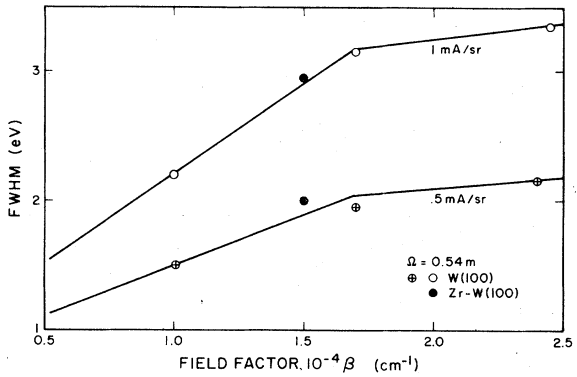

FIG. 14. Experimental values of the FWHM vs the field factor β for $\Omega = 0.54$ msr; upper curve for $I/\Omega = 1$ mA/sr and lower curve for $I/\Omega = 0.5$ mA/sr.

for both the builtup and Zr-W(100) emitters at two values of angular intensity and using the crossover analyzer with $\Omega = 0.54$ mrs.

V. DISCUSSION OF RESULTS

A. Low-temperature results

Because of the extraordinarily high values of field attainable for the W(100) builtup emitter, a relatively large energy range below the Fermi level (noted on the abscissa by E_F) was accessible to the retarding analyzers used in this experiment. For example, the bulge in the TED due to bulk band-structure ramifications occurring at $\epsilon \cong -0.8$ eV, observed previously by Plummer and Gadzuk[29] for emission from the W(100) plane of a thermally-annealed W emitter, is also observed in these studies as shown in Fig. 4. It should be emphasized, however, that in the present case, the (100) crystal plane contains a pyramidal structure[17] with a very small (less than 20 Å) (100) crystal plane at the tip of the pyramid. Apparently, for the latter reason, the surface-sensitive peak in the trailing edge of the TED normally occurring at $\epsilon = -0.35$ eV,[1,29] and believed to be due to surface states,[29,30] does not appear.

Figures 4 and 6 results show that both emitters give experimental TED curves at 84 K, whose deviation from the theoretical curves increase with increasing field. An increase occurs in both the high- and low-energy tails similar to that observed by others,[12,13] except here the increase is at much higher values of J and with a significant effect on the FWHM values as shown in Figs. 8 and 9. Of further significance, is the fact that the experimental values of FWHM increase almost linearly with probe current for both emitters.

The range of fields over which the TED results are obtained is much lower for the Zr-W(100) emitter because of its lower value of work function. Based on Eq. (5), it follows that the current-density range for the Zr-W(100) TED results is 1×10^4 to 6×10^6 A/cm^2, while in the case of the higher-work-function W(100) builtup emitter results we have $J = 4 \times 10^6$ to 4×10^8 A/cm^2. Thus, the TED broadening occurs in a much lower range of J for the lower-work-function emitter.

In terms of the practical considerations as an electron source, it should be pointed out that for a given angular intensity (i.e., I/Ω), the built-up emitter, because of its inherently smaller emitting area, operates at a higher J that the Zr-W(100) emitter. This can be seen in Fig. 15 where the angular intensity versus J is compared for the two emitters with similar values of β. Thus, for similar values of β and angular intensity, the respective values of the FWHM turn out to be nearly identical for the two emitters (See Fig. 14.)

It is instructive at this juncture to inquire as to the cause of the substantial broadening of the TED curves with increasing current. Two mechanisms put forth previously to explain an enhancement of the

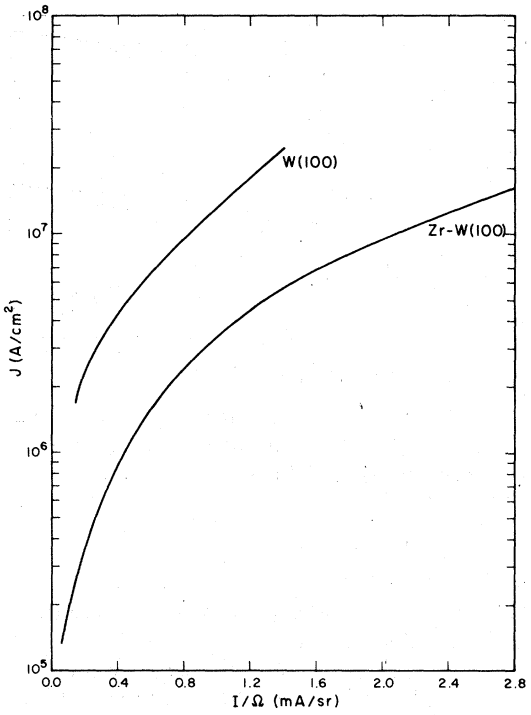

FIG. 15. Curves show the current density J vs angular intensity for the indicated emitters at $T=84$ K, where we have $\beta \cong 1.1\times10^{4}$ cm^{-1} for both emitters.

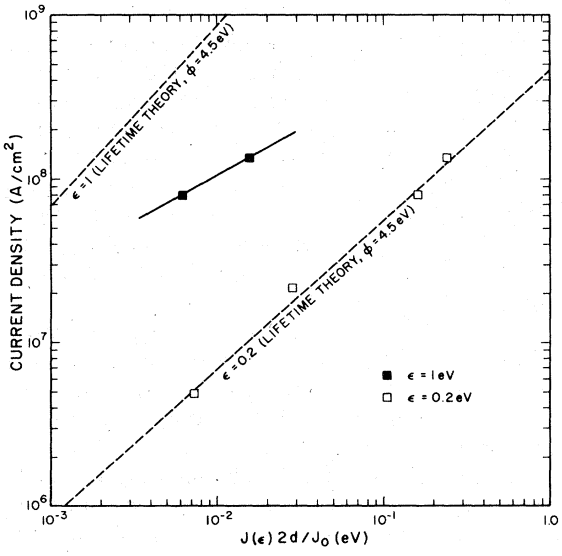

FIG. 16. Experimental values and indicated theoretical curves (dashed lines) of $J(\epsilon)2d/J_0$ vs current density for the W(100) builtup emitter at $T=84$ K and the indicated values of ϵ using the crossover analyzer where we have $\Omega=0.14$ msr.

leading edge of the TED observed for a low-temperature W emitter at much lower values of J are: (i) multiparticle tunneling in which the "hot" holes created by the emitted electrons can decay by Coulomb interaction with a conduction electron leading to a secondary hole and excited electron which has an increased tunneling probability[12,13]; and (ii) lifetime broadening by which the tunneling level width is $\Delta(\epsilon)\cong\hbar/\tau$, where τ is the tunneling time for the bound electron.[14] A level width of the form

$$\Delta(\epsilon)=\Delta_0 e^{\epsilon/d-c}\ , \tag{8}$$

was proposed where Δ_0 is a constant and we have $c=0.68\,\phi^{3/2}v(F,\phi)/F$, where ϕ and F are in units of eV and V/Å, respectively.

The two theories readily predict the ratio of the TED amplitude $J(\epsilon)/J(\epsilon=0)$ [where according to Eq. (3) we have $J(\epsilon=0)=J_0/2d$] which can then be compared with experimental results. Table II gives selected theoretical and experimental values of $J(\epsilon)2d/J_0$ for each emitter at the indicated values of current-density J_0 [calculated from Eq. (5)] and ϵ.

In attempting to compare the experimental results with the two theoretical models, it was found that the lifetime-broadening theory, while failing to agree with the Zr-W(100) emitter TED results using a reasonable value of Δ_0, does agree with the W(100) builtup results at $\epsilon=0.2$ eV using $\Delta_0=0.35$ eV. The agreement between experiment and theory as shown graphically in Fig. 16 is somewhat poorer at $\epsilon=1$ if $\Delta_0=0.35$ eV is used. According to Eq. (8) one obtains a reasonable $\Delta(\epsilon=1)=0.27$ eV for the indicated value of Δ_0 when we have $F=0.79$ V/Å and $\phi=4.5$ eV.

According to Table II, the cascading multiparticle tunneling model, which has no adjustable parameters,[13] fails to agree with the builtup emitter results. This model does exhibit agreement with the Zr-W(100) emitter results at $\epsilon=0.2$ eV. However, this model is inadequate for the following reason: Figures 4 – 7 clearly show that TED broadening occurs on both the high- and low-energy sides of the TED. A similar result was obtained by Gadzuk and Plummer[13] at lower values of J. The multiparticle tunneling model involves a Coulomb interaction between the "hot" holes formed by electron emission and conduction-state electrons, such that the latter are scattered to higher-momentum states prior to tunneling. Thus, this model fails to predict the broadening of the low-energy side of the TED curves. We therefore conclude that another broadening mechanism must be operative in order to explain the Zr-W(100) results and the discrepancy between the lifetime broadening theory and experiment at $J(\epsilon=1)$ for the builtup emitter. Before examining other mechanisms, we shall review the high-temperature results.

TABLE II. Experimental values of $J(\epsilon)2d/J_0$ for the $T=84$ K results are compared with predictions of the two theoretical models of TED broadening.

Emitter	F (V/Å)	J (A/cm^2)	ϵ (eV)	$J(\epsilon)2d/J_0$ Exp	$J(\epsilon)2d/J_0$ Lifetime Broadening[a]	$J(\epsilon)2d/J_0$ Electron Cascade
Zr-W(100)	0.207	3.2×10^5	1.0	5.9×10^{-2}	2.9×10^{-5}	1.0×10^{-3}
Zr-W(100)	0.207	3.2×10^5	0.2	0.55	7.7×10^{-4}	0.34
W(100) buildup	0.79	8.0×10^7	1.0	6.7×10^{-3}	9.4×10^{-4}	0.19
W(100) buildup	0.79	8.0×10^7	0.2	0.16	0.13	50.0

[a]Using $\Delta_0=0.35$ eV.

B. High-temperature results

The high-temperature TED results given in Figs. 5 and 7 for the two emitters show a much larger deviation of the high-energy tail from FN theory. The Zr-W(100) results show a substantial deviation from theoretical expectations on both the high- and low-energy sides of the TED, whereas the W(100) built-up emitter shows a predominant deviation on the high-energy side. As in the case of the low-temperature results, the value of FWHM at elevated temperature increases almost linearly with current as shown in Figs. 8 and 9. The increase of FWHM with beam current is shown dramatically in Figs. 10 to 13 for the two emitters. Figures 12 and 13 show that the near-linear increase of FWHM with beam current is independent of temperature. Even the low-temperature FWHM values approach the high-temperature values at sufficiently high values of beam current (See Figs. 11 and 13).

The Fig. 10 results show that the FWHM values decrease with decreasing β for a specified value of angular beam intensity I/Ω. Curiously, Figs. 11 and 13 show that, for a constant value of β and I/Ω, the FWHM values for both emitters increase with increasing value of beam acceptance angle. For example, in Fig. 12 where we have $\Omega=0.97$ msr, a FWHM value approaching 4 eV was measured at 0.9 mA/sr more than 3 eV above the theoretical expectation!

In addition to the variation of FWHM with Ω, we note that FWHM values for the W(100) builtup emitter shown in Fig. 14, also decrease significantly with increasing emitter radius. Although only one value of FWHM for the Zr-W(100) emitter was obtained in Fig. 14, its value agrees closely with that of the W(100) builtup emitter. According to Fig. 15 at a given value of β and I/Ω, the value of J is considerably larger for the higher-work-function builtup emitter. Thus, the near-identical values of FWHM for the two emitters, as observed in Fig. 14 at a given β and I/Ω, occur at widely differing values of J as well as F. It may be concluded that for a given angular intensity, the higher values of J obtained for the builtup emitter do not lead to higher values of FWHM when compared to the lower-work-function Zr-W(100) emitter, presumably due to a compensating factor such as the increased electric field.

The fact that the builtup emitter exhibits lower values of I/Ω than the Zr-W(100) emitter for the same J, is probably due to the larger beam divergence (i.e, high magnification) from the pyramidal-shaped structure of the builtup emitter.

C. External beam interactions

The fact that anomalous broadening of the TED occurs in data from two different kinds of energy analyzer, one with a high-current density crossover and one without, tends to eliminate analyzer artifacts as a source of the broadening. Since most of the experimental data were obtained from the crossover analyzer, it is worthwhile to estimate the well-known energy broadening which occurs in an electron-beam drift region or at a beam crossover.[20–23,31] Loeffler[20] has calculated a quantity Ω_0 as a function of λr_0, and presented the results in graphical form where Ω_0 is related to the beam energy spread ΔE, due to the crossover according to

$$\Delta E=\frac{1.44\times10^{-7}}{\alpha_0 r_0}\Omega_0\ (\text{eV})\ , \tag{9}$$

where α_0 is the beam half angle in radians, and r_0 is the radius in cm of the crossover; λ is the axial electron density given by

$$\lambda=1.053\times10^{11}I/V_0^{1/2}\ (\text{cm}^{-1})\ , \tag{10}$$

where V_0 is the beam voltage and I is the current in amperes at the crossover. Calculation of lens properties of the crossover analyzer indicates that V_0 is ap-

proximately 0.2 V at the crossover $\alpha_0 \sim 0.1$ rad; and $r_0 \sim 10^{-4}$ cm. Hence we have, $\Delta E \sim 0.014\,\Omega_0$ and $\lambda = 2.35 \times 10^4$ cm^{-1}, i.e., $\lambda r_0 = 2.35$. Loeffler's curves show that at this value of λr_0, we have $\Omega_0 \sim 15$ so that we have $\Delta E \sim 0.21$ V, which, while significant, is still below the experimental values observed in both the crossover and noncrossover analyzers.

While the previously mentioned internal mechanisms of TED broadening can account for a portion of the observed effect, we conclude that an additional mechanism involving electron interaction immediately in front of the emitter is operative. Zimmerman[21] describes a mechanism by which a beam of charged particles, whose initial distribution of velocity between transverse and axial components is changed due to acceleration when viewed in the center of mass coordinate system, can undergo collective interactions at a subsequent crossover or drift space. The latter interaction, which tends to "thermalize" or restore the initial equipartition of velocity components, when viewed in the laboratory frame of reference, leads to a substantial broadening of the initial total energy distribution.

Loeffler[20] has calculated this energy broadening at a beam crossover, as discussed above, and points out that the "electrons contributing most to the energy spread are those that stay closely behind or in front of the reference electron and move almost parallel to it or on only slowly-diverging trajectories." Clearly, the field-emission source itself falls into this category at high values of angular intensity. In his calculations of energy spread, Loeffler assumes a beam crossover with electrons moving through the crossover at constant energy V_0 whereas at the field-emission source, the electrons are rapidly accelerated from a virtual crossover so that acceleration and thermalization occur simultaneously near the emitter. However, it has been found[32] that the same functional relationship derived by Loeffler for a beam crossover holds for the more realistic model of an electron beam accelerated from a spherical source of radius r_0' by a distant anode at V_0. Thus, according to Loeffler, the energy broadening ΔE due to external interactions expressed in terms of beam angular intensity $I' = I/\Omega$ is

$$\Delta E = \pi^{1/2} k(\lambda r_0')(I'/r_0')^{1/2} V_0^{-1/4} \quad , \tag{11}$$

where $k(\lambda r_0')$ is a slowly-varying logarithmic function of λ and r_0'. We can see that ΔE is only weakly dependent on V_0, but more strongly dependent on the ratio I'/r_0'. The experimental dependence of ΔE on I', according to Figs. 12 and 13, supports the square-root dependence predicted by Eq. (11); also, the experimental dependence of ΔE on $\beta \propto 1/r_0'$ according to Fig. 14, conforms with the expectations of Eq. (11).

At constant angular intensity I' Eq. (11) does not predict an increase in ΔE with beam aperture angle, as observed experimentally. Such an effect could be a result of the nonhomogeneous-space-charge potential that decreases with α_0, thereby imparting a greater transverse velocity to those electrons emitted at larger α_0. Since transverse velocity is converted to axial velocity for the field-emitter geometry,[2] the total energy distribution will be broadened by accepting electrons emitted with larger α_0. The fact that a space-charge effect occurs at the high values of J employed here is confirmed both by the deviations observed from the FN equation,[16–18] and an increase in the angular divergence of the electron beam with applied voltage.[17,18]

In conclusion, we note that the broadening of the TED FWHM values measured in this study can be explained by a combination of an internal lifetime broadening mechanism and collective Coulomb interactions, involving transformation between transverse and radial velocity components in the region exterior to the emitter. A knowledge of the exact contributions of the two energy-broadening mechanisms at various values of current density must await further theoretical development, although the results of this study indicate that the external mechanism dominates for $J \gtrsim 10^6$ and 10^8 A/cm^2 where $\phi = 2.5$ and 4.5 eV, respectively.

[1] L. W. Swanson and L. C. Crouser, Phys. Rev. 163, 622 (1967).
[2] J. W. Gadzuk and E. W. Plummer, Rev. Mod. Phys. 45, 487 (1973).
[3] J. J. Czyzeivski, Surf. Sci. 39, 1 (1973).
[4] E. W. Plummer and J. W. Gadzuk, Phys. Rev. Lett. 25, 1493 (1970).
[5] N. J. Dionne and T. N. Rhodin, Phys. Rev. B 14, 322 (1976).
[6] R. H. Fowler and L. W. Nordheim, Proc. R. Soc. London A 119, 173 (1928).
[7] R. H. Good, Jr. and E. W. Müller, Handb. Phys. 21, 176 (1956).
[8] D. R. Penn and E. W. Plummer, Phys. Rev. B 9, 1216 (1974).
[9] N. Nicolaou and A. Modinos, Phys. Rev. B 11, 3687 (1975).
[10] E. W. Plummer and R. D. Young, Phys. Rev. B 1, 2088 (1970).
[11] J. W. Gadzuk, Phys. Rev. B 1, 2110 (1970).
[12] C. Lea and R. Gomer, Phys. Rev. Lett. 25, 804 (1970).
[13] J. W. Gadzuk and E. W. Plummer, Phys. Rev. Lett. 26, 92 (1971).
[14] J. W. Gadzuk and A. A. Lucas, Phys. Rev. B 7, 4770 (1973).

[15]L. W. Swanson, J. Vac. Sci. Tech. 12, 1228 (1975).
[16]J. P. Barbour, W. W. Dolan, E. E. Martin, and W. P. Dyke, Phys. Rev. 92, 45 (1953).
[17]L. W. Swanson and L. C. Crouser, J. Appl. Phys. 40, 4741 (1969).
[18]L. W. Swanson and N. A. Martin, J. Appl. Phys. 46, 2029 (1975).
[19]L. H. Veneklasen and M. Siegel, J. Appl. Phys. 43, 1600 (1972).
[20]K. H. Loeffler and Z. Angew, Phys. 27, 145 (1969).
[21]B. Zimmerman, Adv. Electron. Electron Phys. 29, 257 (1970).
[22]R. W. Ditchfield and M. J. Whelan, Optik (Stuttgart) 48, 163 (1977).
[23]H. Boersch, Z. Phys. 139, 115 (1954).
[24]E. L. Murphy and R. N. Good, Jr., Phys. Rev. 102, 1464 (1956).
[25]A. B. El-Kareh, J. C. Wolfe, and J. E. Wolfe, J. Appl. Phys. 48, 4749 (1977).
[26]W. W. Dolan and W. P. Dyke, Phys. Rev. 95, 327 (1954).
[27]J. W. Gadzuk and E. W. Plummer, Phys. Rev. B 3, 2125 (1971).
[28]P. C. Bettler and F. M. Charbonnier, Phys. Rev. 119, 85 (1960).
[29]E. W. Plummer and J. W. Gadzuk, Phys. Rev. Lett. 25, 1493 (1970).
[30]A. Modinos and N. Nicolaou, Phys. Rev. B 13, 1536 (1976).
[31]J. A. Simpson and C. E. Kuyatt, J. Appl. Phys. 37, 3805 (1966).
[32]R. L. Seliger (private communication).